ELSEVIER

Catalysis Today 82 (2003) 195–206

CATALYSIS TODAY

www.elsevier.com/locate/cattod

PEM fuel cells as membrane reactors: kinetic analysis by impedance spectroscopy

M. Ciureanu [a], S.D. Mikhailenko [b], S. Kaliaguine [b,*]

[a] *H-Power Enterprises of Canada Inc., Montreal, Que., Canada*
[b] *Chemical Engineering Department, Laval University, Ste-Foy, Que., Canada*

Abstract

Proton exchange membrane fuel cells (PEMFC) are considered as electrochemical reactors, performances of which are regarded in the context of the various effects influencing FC output, such as mass transports, kinetic of electrode reactions and charge transfer in polymer electrolyte membrane (PEM). An experimental approach, involving the employment of impedance spectroscopy (IS), which allows a deep insight into the nature of these effects, is discussed and its applications to the different aspects of PEMFC functioning are reported. As examples of the use of IS in PEMFC studies, the investigations of the membrane conductivity and in situ studies of the anode and the cathode processes during FC operation are presented.

Keywords: Proton exchange membrane; Fuel cell; Reactor; Impedance spectroscopy; Mass-transfer

1. Introduction

Polymer electrolyte membrane (PEM) fuel cells must be considered as electrochemical catalytic membrane reactors. Indeed, it can be seen from the scheme of H_2/O_2 PEM fuel cell, shown in Fig. 1, that the proton conducting membrane separates the anode from the cathode compartment, where electrocatalytic oxidation of H_2 and reduction of O_2 occur, respectively. The reaction at the anode is $H_2 \rightarrow 2H^+ + 2e^-$ and at the cathode $4H^+ + O_2 + 4e^- \rightarrow 2H_2O$. Thus, like in any other membrane reactor the performance, measured here in terms of the current generated in the external circuit, depends on the overall outcome of a series of successive steps: mass transport at the anode, surface reaction with charge separation at the anode, proton conduction in the membrane, surface reaction on the cathode and mass transport in the cathode compartment. The usual way to assess this performance is to determine the polarization curve of the cell, which might be as represented in Fig. 2. In such a curve the open circuit potential is always lower than the thermodynamic ideal cell potential. Increasing the cell current also involves a decrease in cell potential. All these drops are associated with the various effects, which affect the steady state rate of the electrochemical reactions, namely the various mass transports, the kinetics of electrode reactions and the resistance to proton conduction in the membrane. Thus the electrochemical analysis of the cell is a means of getting information on the surface reactions at the electrodes. In this study we will focus our attention on the use of an electroanalytical technique of systematic use in current edge research, namely the impedance spectroscopy (IS) in this type of investigations.

* Corresponding author. Tel.: +1-418-656-2708; fax: +1-418-656-3810.
E-mail address: kaliagui@gch.ulaval.ca (S. Kaliaguine).

0920-5861/$ – see front matter © 2003 Elsevier B.V. All rights reserved.
doi:10.1016/S0920-5861(03)00233-5

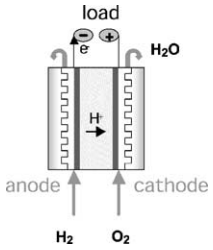

Fig. 1. Schematic illustration of hydrogen–oxygen fuel cell.

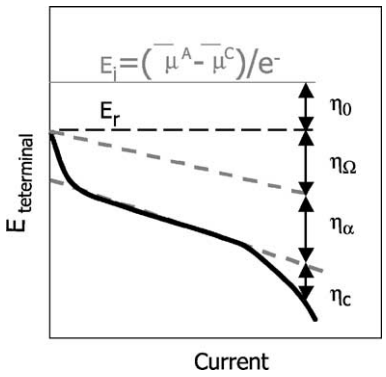

Fig. 2. Current–voltage characteristic of a fuel cell. E_i—ideal cell potential, E_r—rest potential (open circuit), η_O—rest overvoltage, η_Ω—iR, resistance overvoltage, η_a—activation overvoltage, η_C—concentration overvoltage.

2. Principle of IS

AC impedance spectroscopy is a direct method for the study of the various electrochemical processes involved in operation of a PEM fuel cell. It consists in measuring the changes in electrical impedance of a system upon a variation in frequency of an oscillating voltage over a large frequency range (typically 10^{-1} to 10^7 Hz) with modulating voltage of 10–30 mV and bias voltage ranging typically in 0–1 V. The data are reported in the complex plane (Z', Z'') and analyzed after establishing an equivalent circuit to represent the dynamic characteristics of the system. These characteristics are then determined by fitting the impedance data with the equivalent circuit equation using a non-linear least square procedure. In this presentation we will illustrate the multiple uses of this technique as applied to the various parts of a PEM fuel cell. It is in particular indispensable for characterization of PEM and other solid electrolytes and for in situ studies of the anode and cathode processes in the course of FC operation.

3. PEM characterization by IS

Accurate measurement of the proton conductivity σ of electrolyte membranes involves considerable experimental difficulties, associated first of all with the paramount impact of PEM hydration rate on σ. There are a number of experimental approaches to this problem, any of which however has its own advantages and drawbacks. Among various designs of conductivity cells there are:

(a) liquid phase cells where a membrane is equilibrated in a liquid electrolyte solution [1,2] which can obviously affect its chemistry due to ion exchange;
(b) cells where σ is measured in longitudinal direction while membrane surface is exposed to surrounding atmosphere. This allows a sample to be equilibrated with its environment but can produce data quite different from transversal conductivity if bulk properties differ from that of the surface where moisture adsorbs. There are different types of these cells, including frame cells [3–5], classical four point geometry [6,7], coaxial cells [8], etc.;
(c) the most largely used are blocking electrode transversal cells [9–11], where σ can be however underestimated due to difficulties in controlling the membrane water content and problems with specimen–electrode contact;
(d) cells equipped with reversible proton generating electrodes mostly made of Pt-black [12] operating in hydrogen atmosphere. This method is rather complicated and cumbersome for routine measurements.

All these methods (except (d)) have one common feature: they imply using AC IS, which allows to resolve unavoidable electrode polarization effects at the electrolyte–electrode interface. An example of PEM conductivity study by impedance spectroscopy is presented in Fig. 3, where complex responses of a hydrated membrane (sulfonated polyether–etherketone), sandwiched between blocking stainless

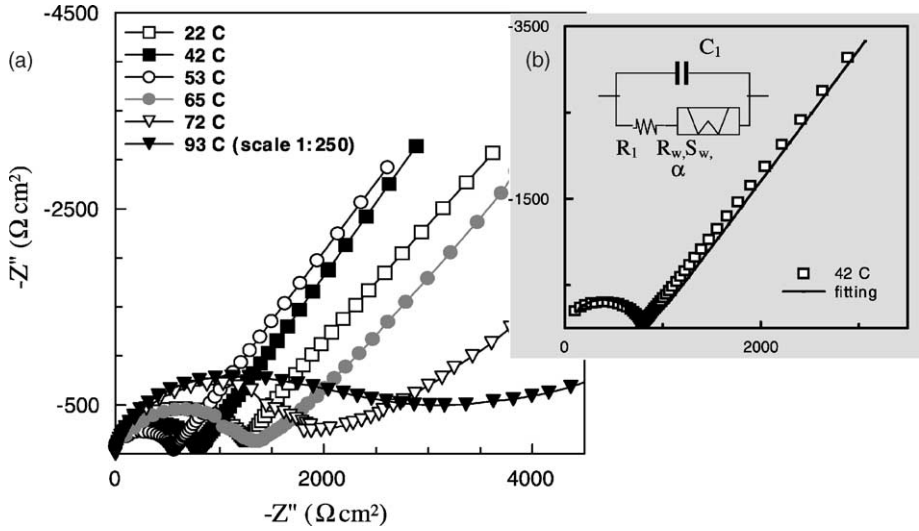

Fig. 3. (a) Typical complex impedance responses of humidified PEM (PEEK, DS = 0.42) at different temperatures. Cell area—1 cm^2, membrane thickness—0.9 mm. (b) Experimental and simulated curves. $R_1 = 640\,\Omega$, $C_1 = 7.5 \times 10^{-11}$ F, $R_w = 600\,\Omega$, $S_w = 6 \times 10^{-4}$ s, $\alpha = 0.32$.

steel electrodes, were recorded as functions of temperature. The spectra consist typically of a low frequency straight line and a high frequency arc, the diameter of which in this instance first decreases with temperature (Arrhenius buildup of conductivity) and then increases following the membrane dehydration. The equivalent circuit, presented in the inset of Fig. 3b, provides a good fit for these responses. It consists of a resistor–capacitor pair ($Z = R_1/1 + iR_1C\omega$) with a generalized Warburg finite length element ($Z = R_w[\coth(iS_w\omega)^\alpha]/(iS_w\omega)^\alpha$) in series with the resistor. Here R_1 represents a bulk resistance of the specimen and C corresponds to the capacitance of the measurement cell. The Warburg element reflects diffusion of charge carriers (protons) within the membrane ($S_w = L^2/D$, where L is the effective diffusion thickness and D the effective diffusion coefficient). The slope of the straight line in the purely diffusional case should be 45° corresponding to $\alpha = 1/2$. The value obtained from fitting $\alpha = 0.32$ for $t = 42\,^\circ$C indicates partially capacitive behavior which becomes still more distinctive with temperature. The best fit for the response at 72 °C, for instance, yielded $\alpha = 0.19$ (not shown in the figure) which is obviously caused by a decrease of the diffusional component with dehydration.

The example presented shows that IS can be useful not only for PEM electrical resistance estimation, but also can provide an important additional information on their behavior depending on the temperature, water content and some other parameters. However still more valuable information can be obtained from IS when it is used for in situ dynamic investigation of full PEMFC.

4. EIS studies of the PEMFC anode

Using IS, it is possible to study separately the electrocatalytic properties of the anode by analyzing the impedance of a half cell which means that in the setup described in Fig. 1 both compartments are fed with hydrogen (H_2/H_2). Alternatively, when studying the effect of CO poisoning, the anode can be fed with a $H_2 + CO$ mixture ($H_2/H_2 + CO$).

CO poisoning of the Pt electrocatalyst is one of the key problems of the PEM fuel cells. Fig. 4 shows the effect of 100 ppm CO in the anode compartment on the polarization curve of a H_2/air PEMFC run at 50 °C (Pt content: 1.7 g/cm^2). For the CO poisoned cell there is a dramatic drop of current at higher voltages. This is followed by a region in which the *I–V* curve

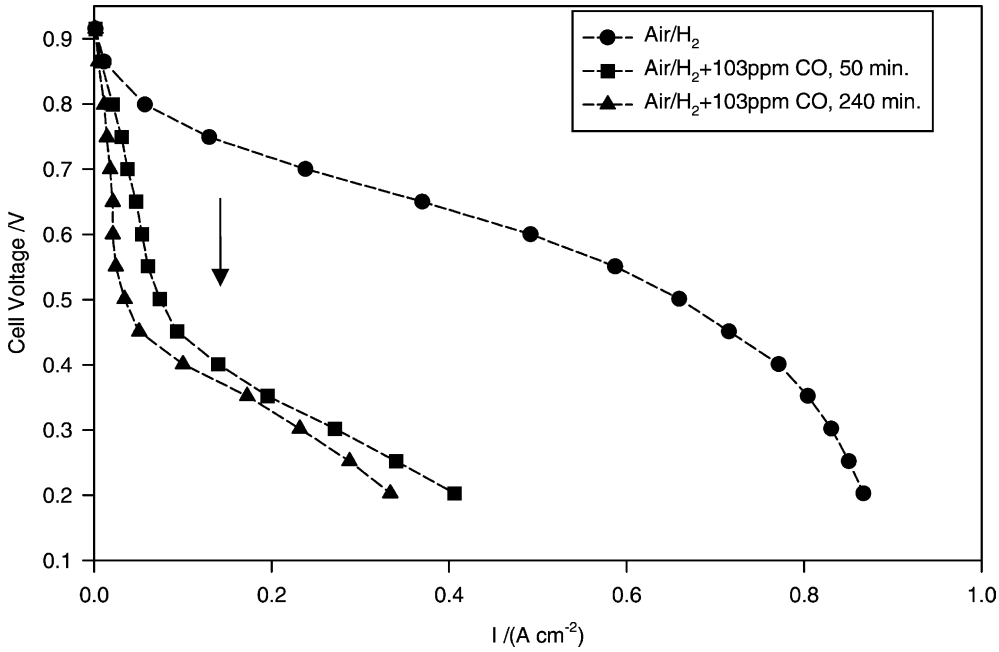

Fig. 4. Polarization curves of H_2/air and $H_2 + CO$/air fuel cell H Power electrodes, 1.7 mg Pt/cm^2, cell temperature: 50 °C; fuel: 80 sccm, 0 psig, 80 °C; air: 600 sccm, 0 psig, by-pass for H_2, 55 °C for $H_2 + 103$ ppm CO. Holding at 0.5 V between measurements.

becomes parallel with that of the unpoisoned cell. The separation between these parallel lines is about 0.45 V. As examples of this type of study we report below two EIS studies of this crucial poisoning effect on Pt/C and Pt + Ru/C electrodes.

4.1. Pt/C electrodes

Fig. 5 shows the complex impedance plot obtained for a symmetrical H_2/H_2 cell at 0.0 V bias potential, whereas Fig. 6 gives the similar impedance patterns of

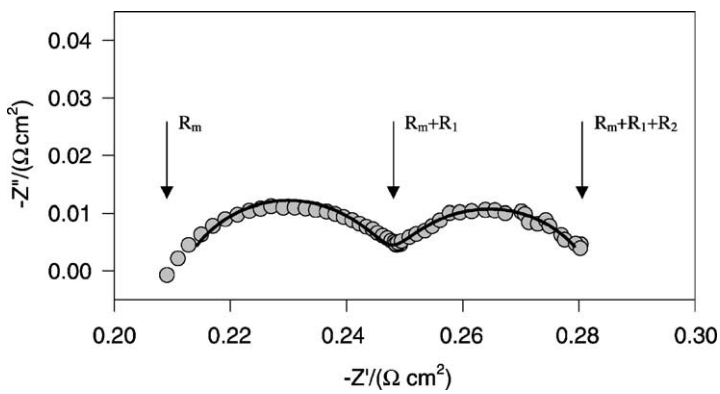

Fig. 5. Impedance plot of symmetrical H_2/H_2 cell at 0.0 V. Points are experimental data, line is a curve fitted with the equivalent circuit of Fig. 7.

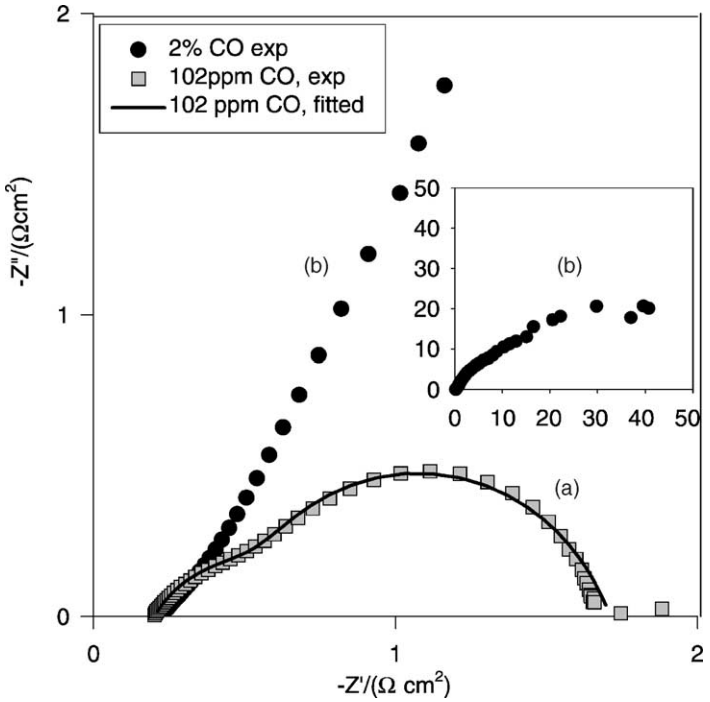

Fig. 6. Impedance patterns at 0.0 V for $H_2/(H_2 + 100\,ppm\,CO)$ cell (a) and $H_2/H_2 + 2\%$ CO (b).

($H_2/(H_2 + 100$ ppm CO)) and ($H_2/H_2 + 2\%$ CO) cells at 0.0 V bias [13]. The equivalent circuit used to represent these data includes a resistance R_m in series with two identical circuits (one for each electrode) each of which is as presented in Fig. 7. In this figure the capacitances C_1 and C_2 used in simulating the (H_2/H_2) cell

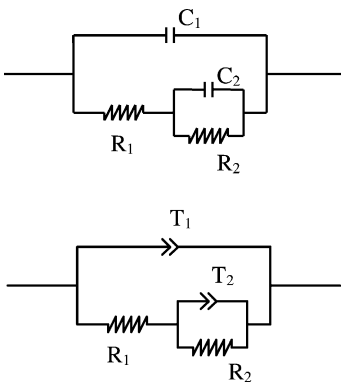

Fig. 7. Equivalent circuits for an electrode with adsorbed species at the interface.

are replaced for the ($H_2/H_2 + CO$) cell with constant phase element (CPE) defined as $Z_{CPE} = 1/[T(j\omega)^{\alpha}]$. Introducing $\alpha < 1$ allows to account for the fact that at high frequency the AC current does not entirely penetrate the pores. The depth of this penetration decreases as ω increases which causes the pore surface area involved to decrease. At low frequency the whole surface is involved, $\alpha \rightarrow 1$ and T becomes the pure capacitance C.

In the data reported in Fig. 5 the high frequency (hf) arc (R_1, T_1) is associated with the charge transfer across the Pt interface ($H_a \rightarrow H^+ + e^-$) and the low frequency (lf) arc (R_2, T_2) with the chemisorption of hydrogen ($H_2 \rightarrow 2H_a$). The lf arc was found not to depend on H_2 flow rate which excludes the possibility that this lf arc would be associated with H_2 diffusion in the porous electrode.

Table 1 reports the values for R_m (membrane resistance), R_1, T_1, α_1, R_2, T_2 and α_2 calculated from the fit of these data. The values of both R_1 and R_2 are drastically increased upon introduction of 100 ppm CO in the gas phase thus monitoring the decrease

Table 1
Parameters evaluated from fit of EIS with the equivalent circuit shown in Fig. 7

Cell	Anode	Bias voltage (V)	R_m (Ω)	R_1 (Ω cm^2)	T_1 (F/cm^2)$^{\alpha_1}$	α_1	R_2 (Ω cm^2)	T_2 (F/cm^2)$^{\alpha_2}$	α_2
H_2/H_2	Pt	0	0.211	0.0181	0.128	0.75	0.0171	30.54	0.70
H_2/H_2 + 102 ppm CO	Pt	0	0.203	0.580	0.026	0.69	0.929	0.035	0.92
H_2/H_2 + 102 ppm CO	Pt/Ru	0	0.201	0.108	0.130	0.65	0.0295	3.444	0.56

in H_a surface concentration associated with CO poisoning. As a confirmation, the EIS spectra reported in Fig. 8 show the time dependence of the measured impedance as the poisoned electrode is flushed with pure hydrogen.

Fig. 9 illustrates the changes in the $H_2/(H_2 + 100\,ppm\,CO)$ cell with bias potential. At low bias (0.1 V) the complex impedance behavior changes only quantitatively showing an increase in the lf limit of the impedance compared to the open circuit (0.0 V) behavior. This is associated with the residual charge transfer indicating partial poisoning of the hydrogen oxidation sites. As the bias potential exceeds 0.291 V a very different spectrum is observed with the lf arc located in the fourth quadrant. This reflects a semi-inductive pattern which was shown to happen in systems with adsorbed species the coverage of which undergoes a change in the sign of its dependence on potential [14]. In the present case this semi-inductive pattern is a proof that the CO coverage starts decreasing at potentials exceeding 0.291 V. The observed drastic decrease in the diameters of the two loops with increasing bias potential up to a $V_{crit} = 0.43$ V, above which the impedance recovers a value close to that

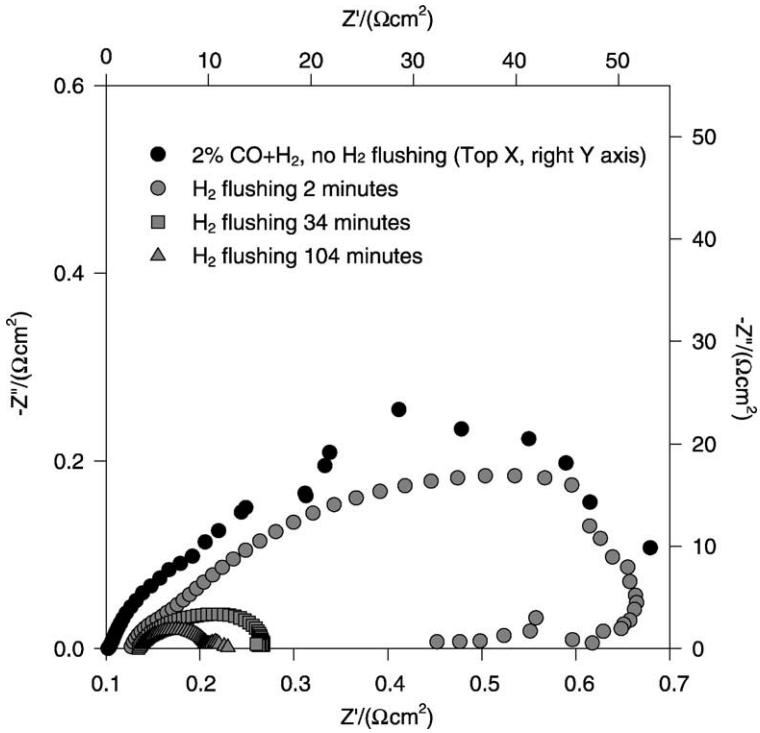

Fig. 8. Complex impedance plot at $E = 0.0$ V for a $H_2/(H_2 + 2\%)$ CO cell after flushing with pure hydrogen for different period of times.

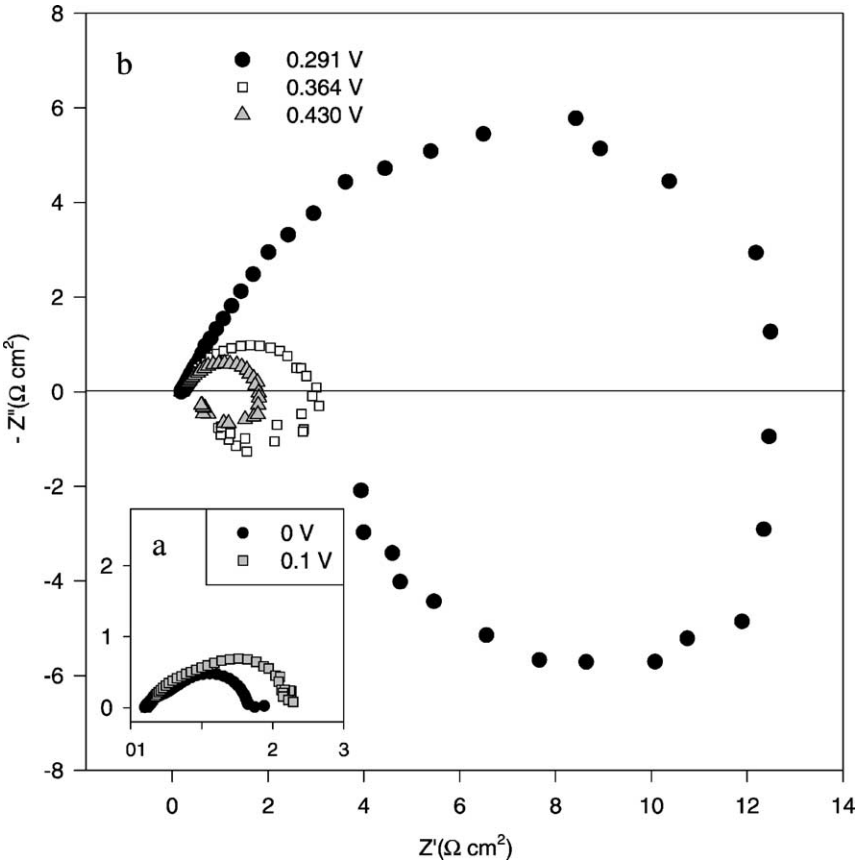

Fig. 9. Influence of the bias voltage (IR corrected) on the complex impedance plot for a $H_2/(H_2 + 100\,ppm\,CO)$ cell: (a) low overvoltage region; (b) high overvoltage range.

of the unpoisoned electrode (a behavior not shown in Fig. 9), reflects the progressive electrochemical depoisoning of the Pt surface by oxidation of adsorbed CO:

$$Pt–CO_{ads} + Pt–H_2O_{ads} \rightarrow 2Pt + CO_2 + 2H^+ + 2e^-$$

This activated water shift is likely since in this bias voltage range there are no $Pt–OH_{ads}$ species on the surface. This process is completed and as mentioned above, the activity of the non-poisoned electrode is recovered as the bias reaches V_{crit}. Reverting to Fig. 4, which shows *I–V* curves of poisoned and unpoisoned systems, it can be seen that these curves are separated by 0.45 V, which is almost exactly identical with the value determined by EIS.

4.2. Pt–Ru/C anode

The complex impedance spectra reported in Fig. 10 [15] were obtained at the 0.0 V bias potential in conditions similar to the data in Fig. 6 except that the Pt anode was replaced with one with a 50% Pt–50% Ru catalyst (3.2 mg/cm^2). The comparison is also shown in Table 1. The lower resistances R_1 and R_2 observed with Pt–Ru compared to Pt electrocatalysts reflect the well known beneficial effect of Ru on Pt deactivation by CO.

The effect of the bias potential on these spectra is represented in Fig. 11. At low bias potential (below 0.3 V) the complex impedance spectrum is similar to the ones observed with the Pt electrodes (see Fig. 8) except for the smaller values of both R_1 and R_2 again

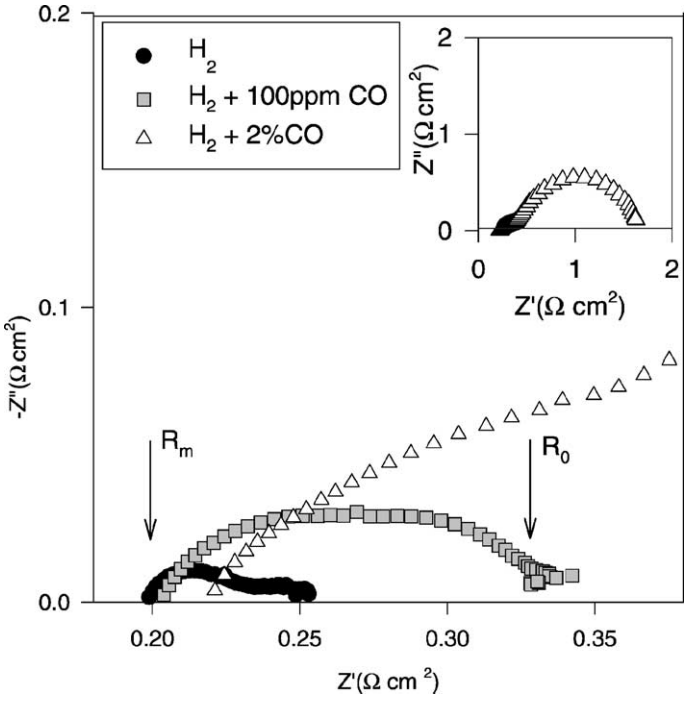

Fig. 10. Open cell complex impedance plots on Pt/Ru based anode.

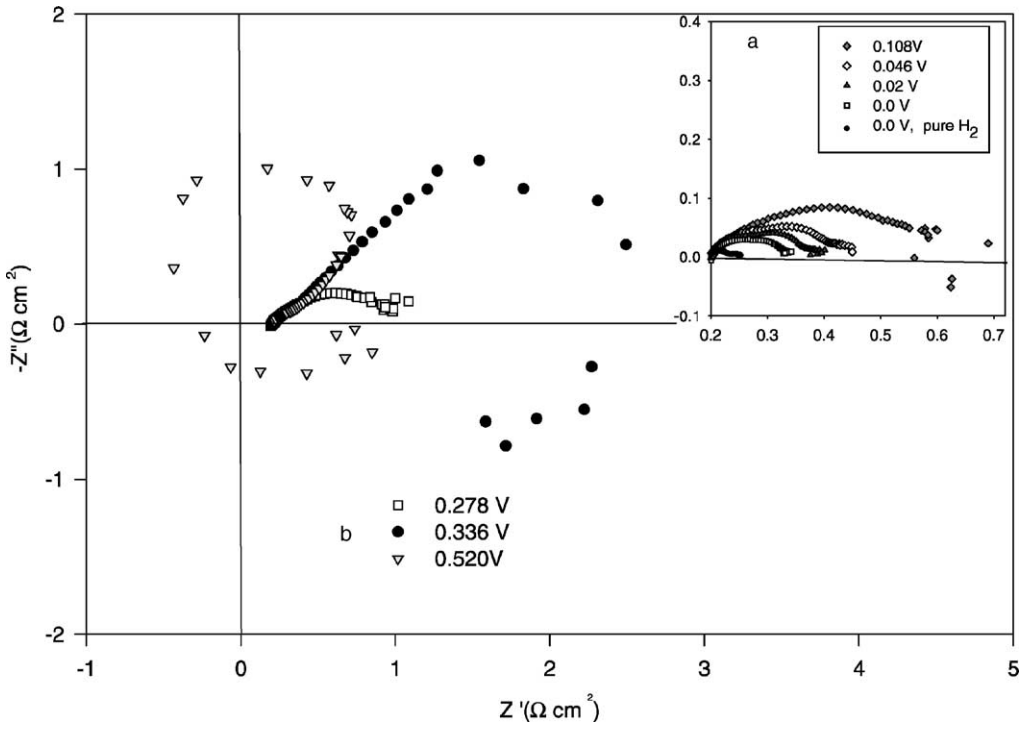

Fig. 11. Complex impedance plot for $H_2/(H_2 + 100\,\text{ppm CO})$ cell at several bias potentials (IR corrected): (a) low overpotential range; (b) high overpotential range.

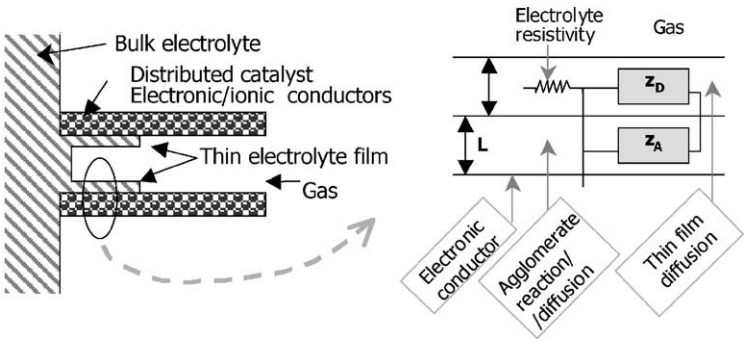

Fig. 12. Agglomerate plus thin-film model of a porous gas diffusion electrode.

indicating a lower degree of CO poisoning. At intermediate bias potential (0.336 V) the curve is also in the fourth quadrant at low frequency indicating a pseudo-inductive pattern. Thus again in these conditions an electrochemical process which removes CO from the surface occurs. Here the reactivation of the surface is assigned to the oxidative removal of CO_{ads} from the surface, in the presence of OH_{ads} species, known to be present on the surface of Ru in this potential range:

$$Pt–CO_{ads}+Ru–OH_{ads} \rightarrow Pt + Ru + CO_2 + H^+ + e^-$$

At the overpotential of 0.52 V an unusual behavior showing two additional arcs in the second and third quadrants is observed which was not given a definite interpretation.

5. EIS studies of the PEMFC cathode

In H_2/O_2 PEM fuel cells it is rather easy to operate in conditions where EIS spectra are essentially determined by the cathode. The interpretation of such spectra is then made on the basis of a model of the porous gas diffusion cathode, the flooded-agglomerate model [16,17], a scheme of which is shown in Fig. 12. The catalyst (usually Pt particles supported on carbon black) is a component of the composite material designated as the agglomerate which acts as a proton conductor, an electron conductor and an oxygen diffuser. This allows the electrode reaction $O_2 + 4H^+ + 4e^- \rightarrow 2H_2O$ to take place on the wetted part of the agglomerate. This part is visualized as covered with an elec-

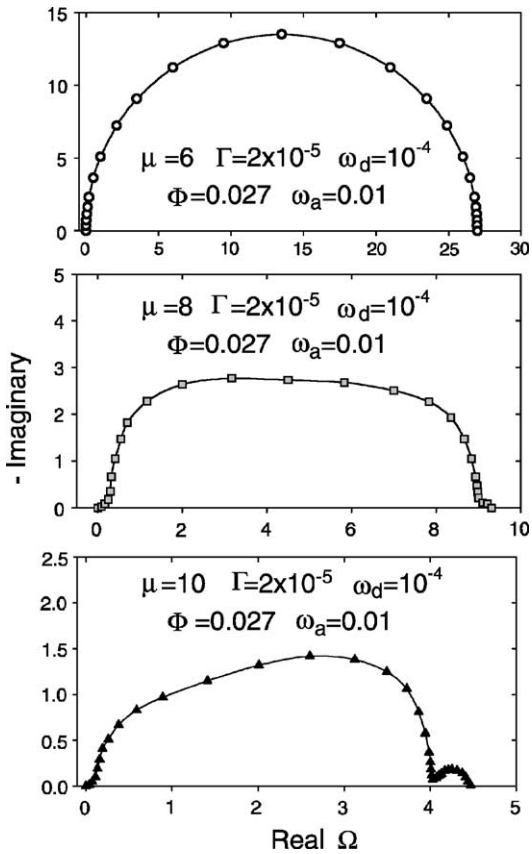

Fig. 13. Response of the complete cathode model (see Fig. 12) as function of potential. The highest frequency arc is caused by double-layer charging, the mid-frequency feature by the agglomerate dynamics, and the lowest frequency process by thin-film diffusion.

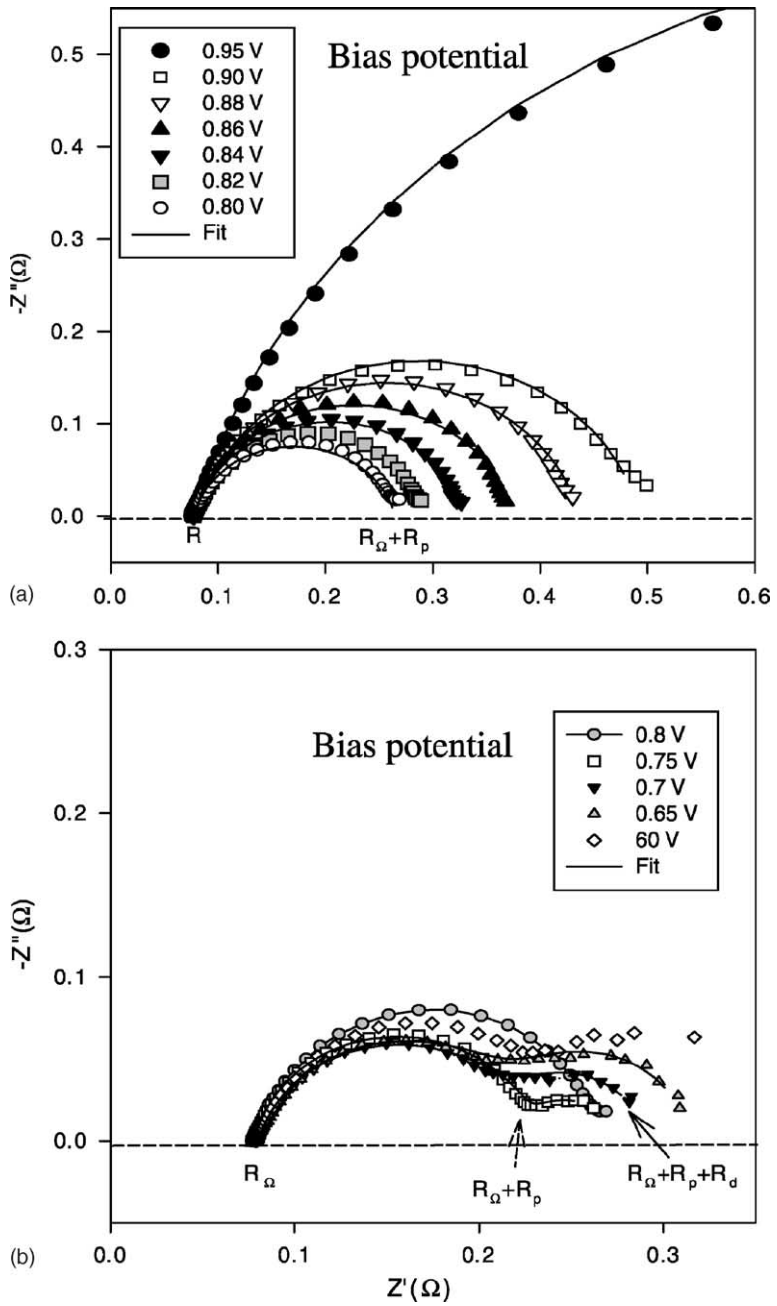

Fig. 14. Experimental potential dependence of the Nyquist plots in the range of 0.9–0.8 V (a) and 0.8–0.65 V (b). $v_{H_2}/v_{air} = 16/40$ sccm, $t_{H_2}/t_{air} = 40/40\,^{\circ}C$.

trolyte thin film through which O_2 from the gas phase must be dissolved and through which it must diffuse. The parameters of this model are shown in Fig. 12. Fig. 13 gives a series of theoretical Nyquist plots for varying values of the parameter $\mu = \eta\alpha F/RT$ where η is the cathode overpotential. The other parameters in these calculations are $\Gamma = k^0\delta/D_f$—film diffusion parameter and $F = (k^0 L_y/D_a)^{1/2}$—agglomerate diffusion parameter, with the effective rate constant k_0 given as $k_0 = k' A_v L_y$ (where k' is true rate constant in cm/s and A_v the catalyst area per unit volume in cm^{-1}).

The characteristic frequencies for thin film ω_f and for agglomerate ω_a are $\omega_f = D_f/\delta^2$ and $\omega_a = D_a/L_y^2$ (in rad/s). Ciureanu and Roberge [18] have obtained experimental data that confirm beautifully the predictions of the flooded-agglomerate model. The EIS spectra shown in Fig. 14a and b were obtained in mild conditions (cell temperature 25 °C and moderate humidification) relevant for the low power fuel cells. The geometric surface area was 25 cm^2, the polymer electrolyte being Nafion 113.5. The electrodes consisted of a thin film of catalyst layer containing 1.7 mg Pt/cm^2, 1% Nafion and 0.4% Teflon. It was hot pressed on a teflonized gas diffusion backing of Toray paper. The electrochemically active electrode surface area as measured by cyclic voltammetry was 200 cm^2/cm^2. At high V_{cath} (low overpotential) comprised between 0.95 and 0.8 V only one loop is observed in the complex impedance plane, with a high frequency intercept R_Ω and a diameter R_p. In this region R_p value decreases rapidly as V_{cath} decreases (Fig. 14). As the voltage decreases below 0.8 V, a second loop appears at low frequency and the first high frequency loop stops varying. From the flooded-agglomerate model, the high frequency loop should be associated with rate of charge transfer at the Pt/electrolyte interface. If this is actually the case, then the R_p value should be related to V_{cath} by the Tafel relationship:

$$V_{cath} = E_0 - b \log R_p^{-1} \quad (1)$$

Eq. (1) was thus tested as shown in Fig. 15, which shows two such curves obtained at two humidification temperatures. It is observed in this figure that each of these curves has three different segments: the one at the highest V_{cath} shows the largest $(-1/b)$ slope and is likely associated with the Pt surface reaction step being rate limiting. As V_{cath} is decreased to values on the order of 0.80 V, a second segment shows a decreased slope, suggesting that the surface process is now coupled with internal O_2 diffusion within the agglomerate layer. Finally at the lowest V_{cath} values, R_p^{-1} is essentially unchanged in coherence with a rate process now limited by the film diffusion process. Indeed, it was observed that the value of R_d (low frequency arc

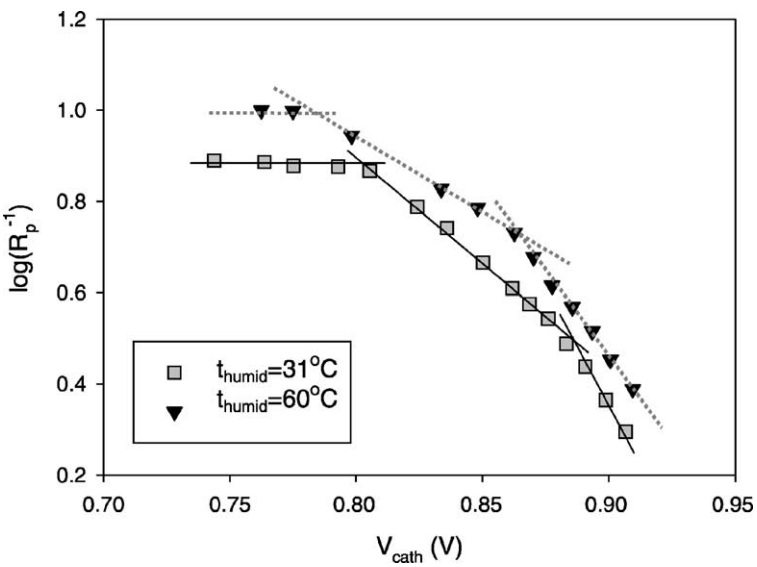

Fig. 15. $\log(R_p^{-1})$ vs. cathode potential at two humidification temperatures $t_{cell} = 25$ °C.

in Fig. 14b) is strongly dependent on the thickness of Toray paper. The general behavior is comparable to the classical behavior of catalytic processes in situations where internal and external diffusion become rate limiting. These results will be further discussed in the presentation as well as other applications of IS to characterization of PEM membranes and analysis of the H_2 anode reaction rates. In particular in this last case we will analyze the poisoning effect of CO on Pt and Pt–Ru anodes.

6. Conclusions

Proton exchange membrane fuel cells (PEMFC) are indeed electrocatalytic membrane reactors, the performances of which are regarded in the context of the various effects influencing FC output, such as mass transports, kinetic of electrode reactions and charge transfer in PEM. Impedance spectroscopy is a powerful tool to study the different process in PEMFC functioning, including investigations of PEM conductivity and in situ studies of the anode and cathode processes during FC operation. The EIS study of anodic processes allowed to monitor the poisoning of the Pt catalyst with CO and its electrochemical reactivation by oxidation of CO_{ads} with $Pt–H_2O_{ads}$ in pure Pt system and with $Ru–OH_{ads}$ in the case of Pt–Ru catalysts. EIS of air cathode evidenced two diffusional processes, interpreted in terms of the flooded-agglomerate model for GDE: a high frequency response reflects interfacial charge transfer and mass transport of oxygen in the pores of the catalyst layer and in a thin electrolyte film. A low frequency response is assigned to the mass transport limitation due to flooding in the backing layer.

References

[1] H.G.L. Coster, T.C. Chilcott, The characterization of membranes and membrane surface using impedance spectroscopy, in: T.S. Sorensen (Ed.), Surface Chemistry and Electrochemistry of Membranes, Marcel Dekker, New York, 1998, pp. 749–792.
[2] W. Cui, J. Kerres, G. Eigenberger, Separ. Purif. Technol. 14 (1998) 145–154.
[3] T.A. Zawodzinki, M. Neeman, L.O. Sillerud, S. Gottesfeld, J. Phys. Chem. 95 (1991) 6040–6044.
[4] J. Zaidi, S.F. Chen, S.D. Mikhailenko, S. Kaliaguine, J. New Mater. Electrochem. Syst. 3 (2000) 27–32.
[5] F. Wang, M. Hickner, Y.S. Kim, T.A. Zawodzinski, J.E. McGrath, J. Membrane Sci. 197 (2002) 231–242.
[6] B.D. Cahan, J.S. Wainright, J. Electrochem. Soc. 140 (1993) L185.
[7] M. Rikukawa, K. Sanui, Prog. Poym. Sci. 25 (2000) 1463–1502.
[8] P.D. Beattie, F.P. Orfino, V.I. Basura, K. Zychowska, J. Ding, C. Chuy, J. Schmeisser, S. Holdcroft, J. Electroanal. Chem. 503 (2001) 45–56.
[9] P. Staiti, F. Lufrano, A.S. Arico, E. Passalacqua, V. Antonucci, J. Membrane Sci. 188 (2001) 71–78.
[10] L. Depre, M. Ingram, Ch. Poinsignon, M. Popall, Electrochim. Acta 45 (2000) 1377–1383.
[11] T. Kobayashi, M. Rikukawa, K. Sanui, N. Ogata, Solid State Ion. 106 (1998) 219–225.
[12] E. Skou, I.G.K. Andersen, E.K. Andersen, D.c. techniques and ac/dc combination techniques, in: Ph. Colomban (Ed.), Proton Conductors. Solids, Membranes and Gels—Materials and Devices, Cambridge University Press, Cambridge, UK, 1992, pp. 418–431.
[13] M. Ciureanu, H. Wang, J. Electrochem. Soc. 146 (1999) 4031–4040.
[14] L.J. Gao, B.E. Conway, J. Electroanal. Chem. 395 (1995) 261.
[15] M. Ciureanu, H. Wang, Z. Qi, J. Phys. Chem. B 103 (1999) 9645–9657.
[16] T.E. Springer, I.D. Raistrick, J. Electrochem. Soc. 136 (1989) 1594–1603.
[17] I.D. Raistrick, Electrochem. Acta 35 (1990) 1579–1586.
[18] M. Ciureanu, R. Roberge, J. Phys. Chem. B 105 (2001) 3531–3539.